EVALUATION OF VERTICAL PROFILES OF DUST CONCENTRATIONS FROM THE MONARCH OPERATIONAL FORECAST

BDRC-2025-002

Carlotta Gilè, Jeronimo Escribano, Emanuele Emili,
Oriol Jorba, Carlos Pérez García-Pando*
Barcelona Supercomputing Center, BSC
(*) Catalan Institution for Research and Advanced Studies, ICREA
Ernest Werner, Gerardo García-Castrillo
Spanish State Meteorological Agency, AEMET

29 July 2025

TECHNICAL REPORT

Series: Barcelona Dust Forecast Center (BDRC) Technical Report

A full list of BDFC Publications can be found on our website under: http://dust.aemet.es/about-us/technical-reports

C/Jordi Girona, 29 | 08034 Barcelona (Spain)

Summary

This document presents the first evaluation of a new forecast product disseminated by the Barcelona Dust Regional Center (BDRC) since July 2024, namely the vertical profiles of dust concentrations from the MONARCH model. The assessment has been done by comparison with lidar measurements from the NASA Micro-Pulse Lidar Network (MPLNET) across three sites in the Mediterranean and North Africa from July 2024 to April 2025. To compare simulated dust concentrations with lidar measurements the following two steps have been carried: i) the estimation of the dust contribution to the total aerosol extinction from MPLNET Level 2 (L2) products ii) the computation of dust extinction profiles from the publicly available forecast products (dust optical depth, dust load, and dust concentration profiles). This preliminary evaluation was conducted by examining correlations over time between model 24-hour forecasts and lidar measurements, and additional metrics such as the average dust layer height. Reasonable agreement has been found between simulated and measured vertical profiles of mineral dust, demonstrating capabilities of forecasting main features of dust vertical distribution.

Contents

1. Data and Methodology

1.1. Model Data

The Multiscale Online Nonhydrostatic AtmospherRe Chemistry model (MONARCH), developed at the Barcelona Supercomputing Center (BSC), is an online meteorology-chemistry model that provides short- and mid-term chemical weather forecasts on both regional and global scales (Pérez et al., 2011; Haustein et al. 2012; Jorba et al. 2012; Spada et al. 2013; Spada et al. 2015; Badia and Jorba 2015; Badia et al. 2017; Di Tomaso et al. 2017; Xian et al., 2019; Klose et al., 2021). MONARCH is based on the online coupling of the meteorological Nonhydrostatic Multiscale Model on the B-grid (NMMB; Janjic and Gall, 2012) developed at the National Centers for Environmental Prediction (NCEP), with a full chemistry module, including gas phase and all aerosol species, developed at the BSC. Therefore, the model is designed to account for the feedback among gases, aerosol particles, and meteorology. The aerosol module is enhanced with a data assimilation (DA) system to optimally combine forecasts with observations and improve predictions (Di Tomaso et al. 2017; Di Tomaso et al. 2022; Escribano et al., 2022).

The desert dust module, previously known as NMMB/BSC-Dust (Pérez et al., 2011) that is embedded into the NMMB meteorological core, solves the mass balance equation for dust taking into account the following processes: i) dust generation and uplift by the wind, ii) horizontal and vertical advection, iii) horizontal diffusion and vertical transport by turbulence and convection, iv) dry deposition and gravitational settling, v) wet removal, including in-cloud and below-cloud scavenging. The MONARCH model is the reference model of the WMO Barcelona Dust Regional Center, while the model also contributes to the WMO SDS-WAS regional dust multi-model ensemble, the Copernicus Regional air quality multi-model ensemble, and the ICAP global operational aerosol multi-model ensemble.

The resolution of the model is set to 0.10º x 0.10º, covering North Africa, Middle East and Europe (NAMEE, domain) and 40 layers vertically (top of the domain at 50hPa). The Global Forecast System (GFS) at 0.5º x 0.5º and produced at 12 UTC by the National Centers for Environmental Prediction (NCEP) is used as initial meteorological conditions and boundary conditions at intervals of 6 h. The simulated dust distributions consist of daily runs of 84-hour forecast length, and the initial state of the dust concentration is defined by the 24-h forecast of the previous-day model run. Only in a ‘cold start’ of the model, the concentration is set to zero.

Vertical layers of dust concentration describe how the concentration of dust particles varies with altitude in the atmosphere. These profiles are essential in understanding dust transport, radiative forcing, and surface deposition, and they influence visibility, air quality, and cloud microphysics (Mamali et al. 2018). Since July 2024, vertical profiles of dust concentrations have been displayed daily on the BDRC website. The model outputs 3-hourly forecasts of 13 vertical levels defined in meters above sea level: 250, 500, 750, 1000, 1500, 2000, 3000, 4000, 5000, 6000, 8000, 10000, and 12000 m.

To derive the dust extinction, which is the quantity that will be evaluated in this report, three

outputs of the models have been exploited:

- Dust concentration (μg/m³): mass concentration of dust at each vertical level.
- Dust load (g/m²): Total mass concentration of dust in the vertical column of the atmosphere.
- Dust optical depth (unitless): column-integrated dust extinction coefficient.

We computed the dust extinction coefficient (α_{dust}) of the model from the dust concentration ($concdu$), the dust load ($loaddu$), and the dust optical depth ($od550du$) in the following way:

$$\alpha_{dust}(z) = \frac{od550du}{loaddu} \cdot concdu(z) \quad \left[\frac{m^2}{kg} \cdot \frac{kg}{m^3} = \frac{1}{m}\right]$$

The BDRC provides MONARCH dust concentrations at a subset of model levels z, the dust load, and the dust optical depth. We then compute the $\alpha_{dust}(z)$, assuming it is directly proportional to the $concdu(z)$, and scale it by $\frac{od550du}{loaddu}$, to ensure that the integrated extinction matches the model's $od550du$. This is a simplification concerning the actual modeled extinction $ec550du(z)$, which takes into account aerosol microphysical properties, the refractive index, and environmental parameters like relative humidity (Pérez et al., 2011). Our method neglects the vertical variability of these properties because it only relies on the total concentration of dust and therefore provides only an approximate reconstruction of the actual dust extinction profile.

1.2. Lidar Data: MPLNET

The NASA MPLNET network (Welton et al., 2001), which has been operational since 1999, consists of a global network of ground-based lidar instruments designed to measure aerosol and cloud vertical structure and boundary layer heights. The devices are micropulse lidars (MPLs) manufactured by LEICA Geosystems in Lanham, Maryland, USA (previously SigmaSpace, Welton et al. 2001). The data is collected continuously, every 60 seconds, from the surface up to a height of 30 km, with a software-adjustable vertically resolved spatial resolution (30-75 m, depending on the station) and at a wavelength in the range of 523-532 nm (Welton et al. 2001). Temporary and permanent observational sites are installed globally and sometimes, where possible, co-located with the NASA Aerosol Robotic Network (AERONET) sunphotometers to reduce retrieval errors (Welton et al. 2002). MPLNET products are publicly available on its website.

For our analysis, we used the following L15 products:

- Total extinction coefficient (km^{-1}, α_{tot})
- Total backscatter coefficient (km^{-1}, β_{tot})
- Total particle linear depolarization ratio (PLDR, unitless, δ_{tot})

The last two were needed to derive the dust component from the total extinction coefficient.

Figure 1.1 depicts the vertical structure and temporal evolution of aerosols and clouds in the atmosphere. Specifically, the total aerosol backscatter, the mixed layer top, and some cloud phase types (ice, water, mixed, unknown) are shown in El Arenosillo on the 15th of May 2025. The backscatter is represented on a logarithmic scale (km^{-1} sr^{-1}). The brown line depicts the mixed layer top. It indicates the estimated planetary boundary layer height (PBLH), the layer in which most near-surface dust and aerosols are confined.

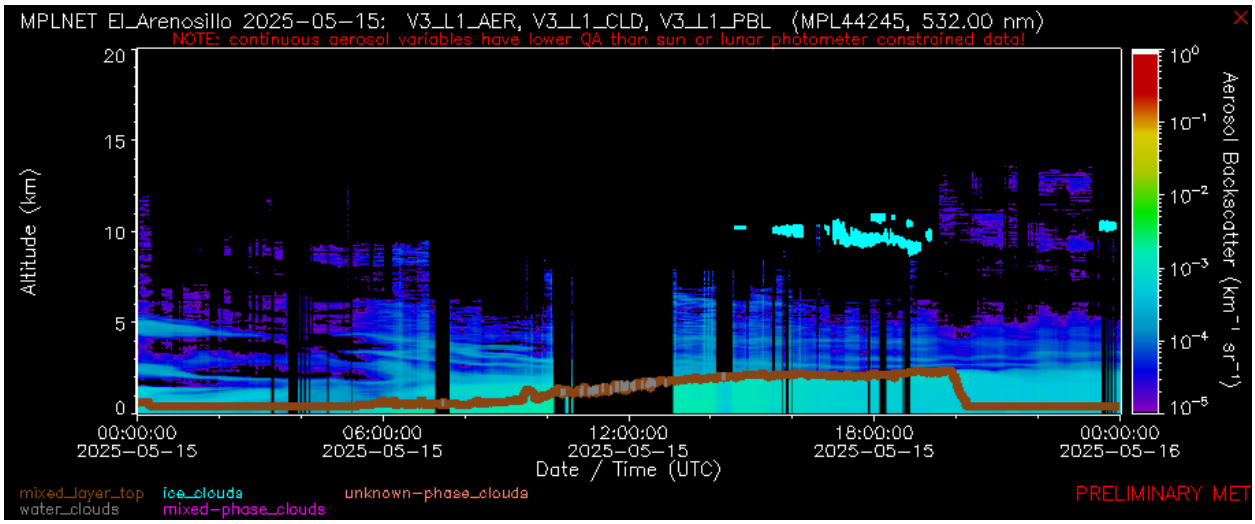

***Figure 1.1**: Picture taken from the MPLNET website depicting the time series of aerosols and clouds in El Arenosillo on the 15th of May 2025. The main variable shown is the aerosol backscatter coefficient.*

MPLNET data has been filtered to remove low-quality and failed retrievals, exploiting several quality control flags provided in the datasets (see MPLNET Product Page: AER). Each flag represents a particular screening criterion. The flag values follow a hierarchical coding scheme (e.g., 1B, 2B, 4B, etc.) where higher values indicate a worse retrieval or data with lower quality.

For our analysis, we used the following flag thresholds:

- `flag_cloud_screen` > 1. This flag identifies the presence of clouds in the observed atmospheric column. Values greater than 1B reflect varying degrees of cloud contamination.
- `flag_cloud_screen` > 1. This flag identifies the presence of clouds in the observed atmospheric column. Values greater than 1B reflect varying degrees of cloud contamination.
- `flag_inversion` > 1. This flag captures the success of the aerosol inversion process. Only samples with no issues were included in the analysis.
- `flag_layers` > 1. This flag is used to indicate failure to detect aerosol layers. Samples with `flag_layers` = 1 (no issues) were considered valid.
- `flag_aod` >= 8. This flag describes the source and quality of the aerosol optical depth (AOD) constraint used in the retrieval. Only failed AOD retrievals were removed.
- `quality assurance (qa) flags` >= 8. Only data with QA flags below the failure

threshold were retained.

This screening was necessary to ensure that only cloud-free profiles with successful inversions were used in the analysis. However, we needed to maintain a balance between data quality and sample availability, and that explains why we did not apply stricter thresholds in the quality assurance and AOD flags.

1.3. Dust Extinction Retrieval

To derive the dust fraction of the total extinction coefficient for MPLNET, we used the POLIPHON algorithm (Tesche et al. 2009). The algorithm decouples the dust component from the total aerosol extinction by using the total backscatter coefficient, the total PLDR, and by making some assumptions regarding the dust lidar ratio ($S_{\lambda,d}$), the non-dust PLDR ($\delta_{\lambda,nd}$), and the dust PLDR ($\delta_{\lambda,d}$):

$$\alpha_{\lambda,d}(z) = S_{\lambda,d} \cdot \beta_{\lambda,d}(z) \quad \left[\frac{1}{km}\right]$$

$$\beta_{\lambda,d}(z) = \beta_{\lambda,p}(z)\frac{(\delta_{\lambda,p}(z) - \delta_{\lambda,nd})(1+\delta_{\lambda,nd})}{(\delta_{\lambda,d} - \delta_{\lambda,nd})(1+\delta_{\lambda,p}(z))} \quad \left[\frac{1}{km}\right]$$

Where α and β are the extinction and backscatter coefficients, z is the altitude, λ is the wavelength (532 nm), and the subscripts "d", "nd", and "p" stand for "$dust$", "$non-dust$", and "$particle$" (total) respectively.

Following Proestakis et al. 2025 we made the following assumptions:

- Dust PLDR, $\delta_{\lambda,d} = 0.31$
- Non-dust PLDR, $\delta_{\lambda,nd} = 0.05$
- Dust lidar ratio, $S_{\lambda,d} = 56$ sr

We assumed these values to be constant, being aware of the fact that the optical properties of aerosols, including the particle depolarization ratio and lidar ratio, can vary with location, altitude, aerosol type, and atmospheric conditions, which may introduce uncertainties in the retrieved dust extinction profiles (Ansmann et al 2017, Ansmann at al 2019).

Moreover, since the $\beta_{\lambda,d}(z) =$ must be lower than or equal to the $\beta_{\lambda,p}(z)$, we imposed:

$$0 \leq \frac{(\delta_{\lambda,p}(z) - \delta_{\lambda,nd})(1+\delta_{\lambda,nd})}{(\delta_{\lambda,d} - \delta_{\lambda,nd})(1+\delta_{\lambda,p}(z))} \leq 1$$

Figure 1.2 shows the total extinction coefficient together with the dust extinction coefficient derived with the POLIPHON algorithm in Tenerife on the 14th of July 2024, around 1:30 AM. Below 1 km, other types of aerosols like sea salt are correctly filtered out, while, instead, some non-dust residuals appear at higher altitudes. This outcome is consistent with some limitations

of the POLIPHON algorithm, which extracts the dust component by using fixed assumptions on the dust lidar ratio, the dust, and the non-dust PLDR. The algorithm does not attempt to retrieve other types of aerosols, such as sea salt or smoke, which can also be present in the observed vertical column.

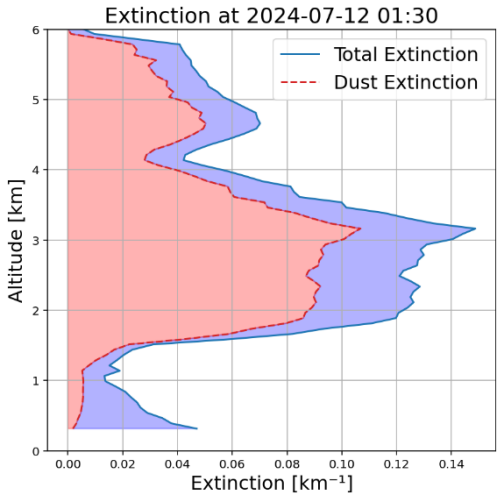

***Figure 1.2**: Total and dust extinction coefficients in Tenerife on the 14th of July 2024 at 1:30 AM.*

From the calculated dust extinction, it was possible to retrieve the dust optical depth (DOD) as:

$$DOD = \int_{z_{min}}^{z_{max}} \alpha_d\,(z)\,dz$$

where z represents the altitude and $\alpha_d\,(z)$ the dust extinction.

In addition to the computation of the DOD, we also used the dust extinction to estimate the average altitude of the dust layer, which provides a compact descriptor of the vertical position of the dust plume. The dust layer height was computed for both the model and the lidar data according to Kylling et al. 2018:

$$z = \frac{\sum \alpha_i\, z_i}{\sum \alpha_i}$$

where $z_i$represents the height of the i-th layer and α_i the dust extinction coefficient at that altitude.

The dust layer height is identical to the real center of mass (COM) when particle composition and size distribution remain constant with altitude. The center of mass represents the height where the majority of the dust load is concentrated (Mona et al. 2006).

1.4. Spatio-Temporal Collocation

As shown in Figure 1.3, we selected three MPLNET stations: Barcelona (41.3860° N, 2.1170° E), El Arenosillo (37.1050° N, 6.7340° W), and Tenerife (28.4720° N, 16.2470° W). For each day between July 2024 and May 2025, we selected the closest MONARCH grid point to each MPLNET station and extracted the vertical dust concentration profile, the dust load, and the dust optical depth. MPLNET dust extinction was temporally averaged every 3 hours to match the MONARCH forecast frequency. The dust optical depth was then calculated from the averaged samples.

***Figure 1.3**: Google Maps view of the three sites under study.*

The MPLNET vertical resolution spans 400 altitude levels, whereas MONARCH defines 13 altitude bins from 250 m to 12 km. To enable direct comparison between the two dust extinction parameters, we vertically averaged the high-resolution MPLNET profiles to the coarser MONARCH vertical grid. The resulting regridded MPLNET dust extinction matched the 13 discrete altitude levels of the MONARCH model, enabling vertical correlation analysis.

2. Results

2.1. Time Series

Figures 2.1, 2.3, and 2.5 show the comparison of the vertical profiles of MONARCH (blue dashed lines) and MPLNET (green solid lines) dust extinction at the three sites at 3-hour intervals during some dust episodes. The average height of the dust layer of the two datasets is also depicted in the plots. We focused our analysis on dust events, which we identified based on the MPLNET DOD. We only retained those time samples for which the $DOD \geq 0.02$, to ensure the presence of appreciable dust concentration.

In Figures 2.2, 2.4, and 2.6, the temporal variability of the dust optical depth of both MONARCH and MPLNET is depicted. Only the months corresponding to the dust episodes selected and presented in this report are shown.

The dust episode in Barcelona on the 16th and 17th of February 2025 (Figure 2.1) depicts an example of overestimation of the dust layer. The vertical shape of the profiles does not vary significantly during the two days. MONARCH tends to overestimate the dust extinction, especially at the end of the first day and during the first half of the second day. There was no lidar data at the beginning of the 16th of February. The plot in Figure 2.2 depicts how the lidar sees a more or less constant DOD with a layer height lowering in time. In contrast, MONARCH seems to detect two dust plumes, one reaching its maximum at 9:00 on the 16th of February and the other one reaching its maximum at 3:00 on the 17th of February, and with a greater magnitude of more than 0.20.

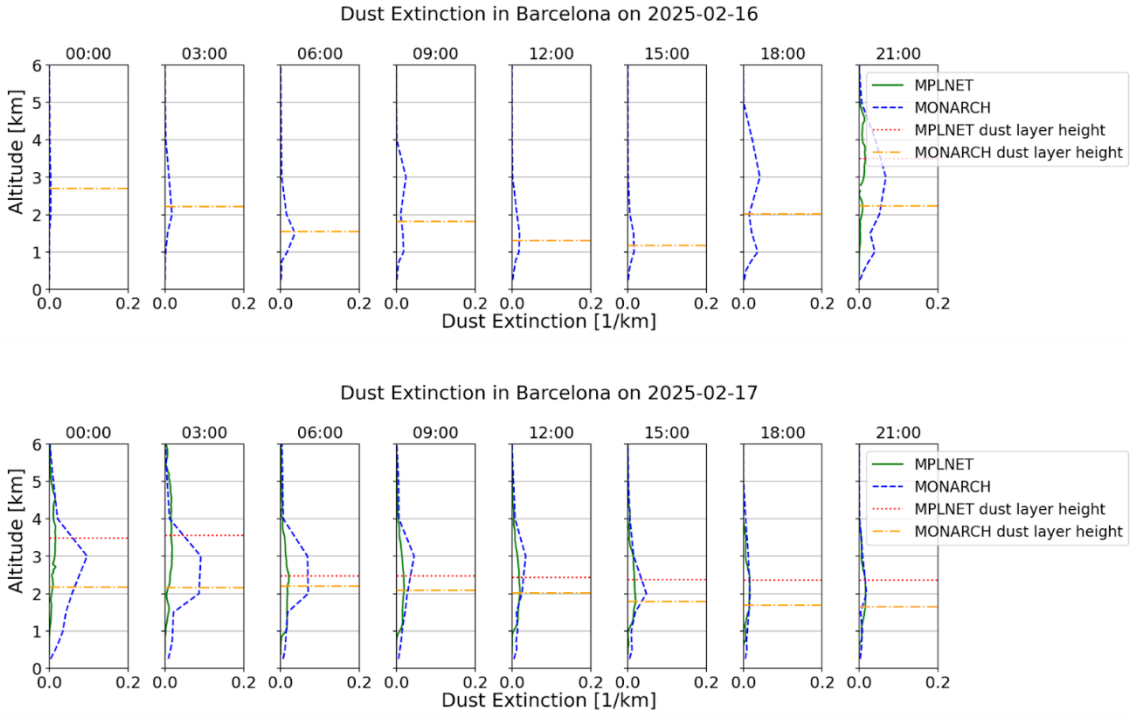

***Figure 2.1**: Comparison of MONARCH and MPLNET dust extinction in Barcelona during the 16th and 17th of February 2025.*

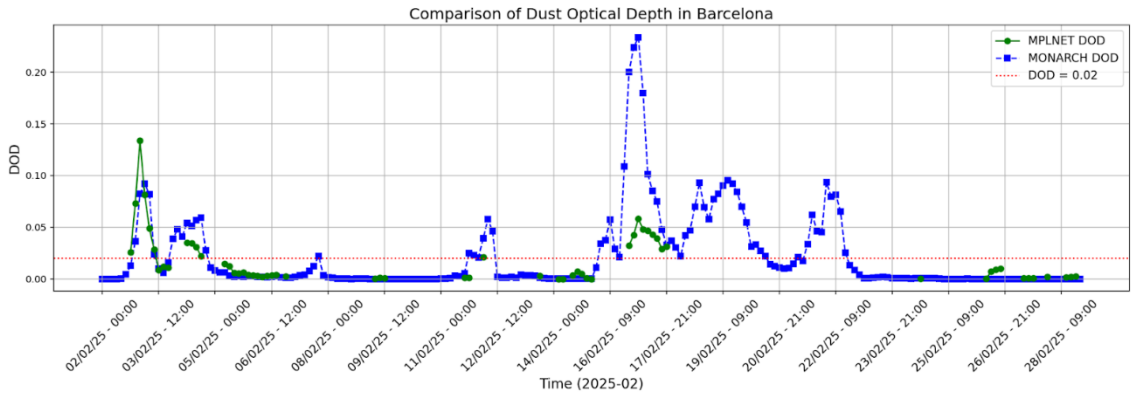

***Figure 2.2**: Time evolution of MONARCH (blue curve) and MPLNET (orange dashed curve) dust optical depth in Barcelona. The red dotted line represents the threshold we used to identify the dust events.*

Figure 2.3 identifies a dust episode in El Arenosillo on the 15th and 16th of September 2024. During the first day, the model and the lidar data exhibit good agreement in the magnitude of the dust layer. Nevertheless, MONARCH retrieves the dust plume at higher altitudes compared to the MPLNET results. On the 16th of September, the dust plume becomes more pronounced in MPLNET measurements, and MONARCH correctly captures this behavior. Although MONARCH evaluates the dust layer at the same altitude and with the same vertical extent, it underestimates the magnitude of the dust extinction. This is further confirmed by the comparison of DOD values (Figure 2.4): on the 15th, both MPLNET and MONARCH show similar DOD values with peaks around 0.05. However, on the 16th, MPLNET records a sharp peak in DOD reaching ~0.35, while MONARCH oscillates around 0.12. This underestimation of DOD is

consistent with the lower extinction values seen in MONARCH's vertical profiles during that day.

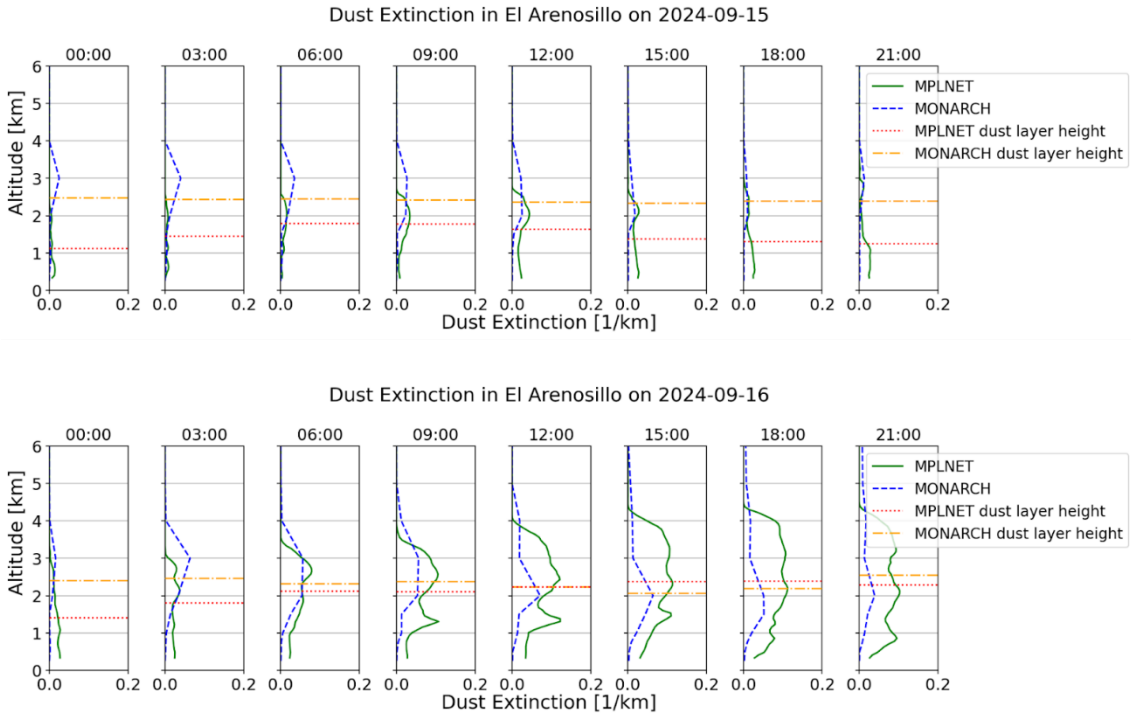

***Figure 2.3**: Comparison of MONARCH and MPLNET dust extinction in El Arenosillo during the 15th and 16th of September 2024.*

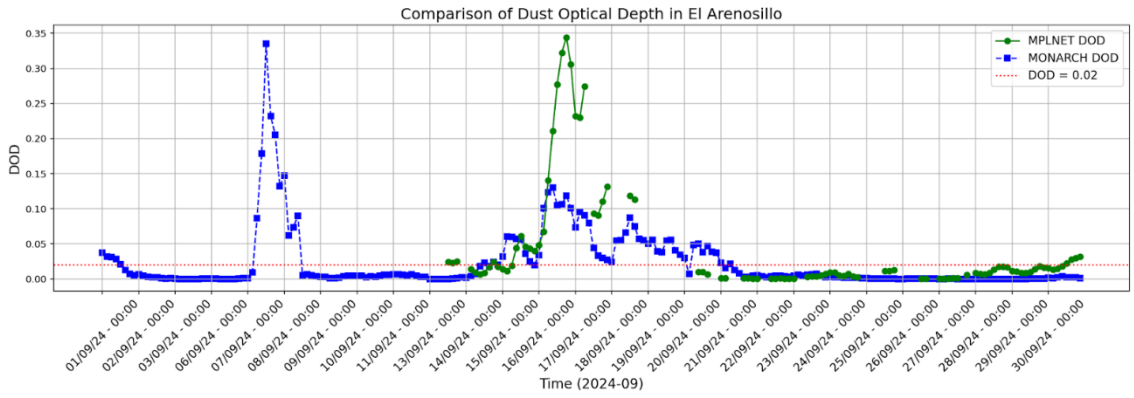

***Figure 2.4**: Time evolution of MONARCH (blue curve) and MPLNET (orange dashed curve) dust optical depth in El Arenosillo. The red dotted line represents the threshold we used to identify the dust events.*

The Tenerife dust episode on the 14th and 15th of July 2024 (Figure 2.5) showcases an example of the overall good agreement between the lidar data and the model data. In the first half of July 14th, MPLNET detects a prominent dust layer extending from approximately 1 km to 5 km. Within this layer, two distinct extinction peaks are located, with a maximum value of the extinction exceeding 0.2 km^{-1}. MONARCH captures the vertical extent and structure fairly well but, underestimates the lower-altitude peak and overestimates the upper peak a bit. On July 15th, the dust plume appears to be more elevated (2-6 km), and this upward shift is consistently

represented in both MONARCH and MPLNET results. MONARCH shows better agreement with MPLNET in both magnitude and structure, especially between 15:00 and 21:00, although some overprediction remains.

Figure 2.6 confirms the general good agreement by showing that the MPLNET and MONARCH DOD curves have comparable patterns. On the 14th of July, MONARCH slightly overestimates the DOD (with values around 0.9) compared to MPLNET (peaking around 0.7). On the 15th of July, the difference persists, but both datasets exhibit a gradual decline in DOD.

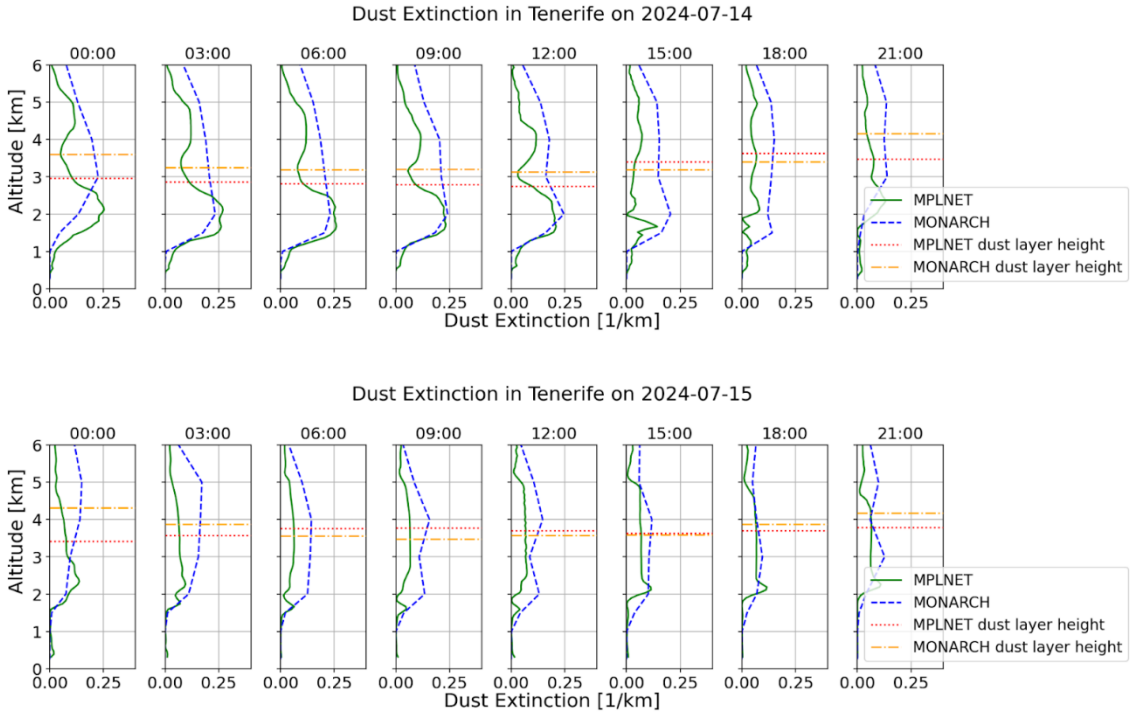

***Figure 2.5**: Comparison of MONARCH and MPLNET dust extinction in Tenerife during the 14th and 15th of July 2024.*

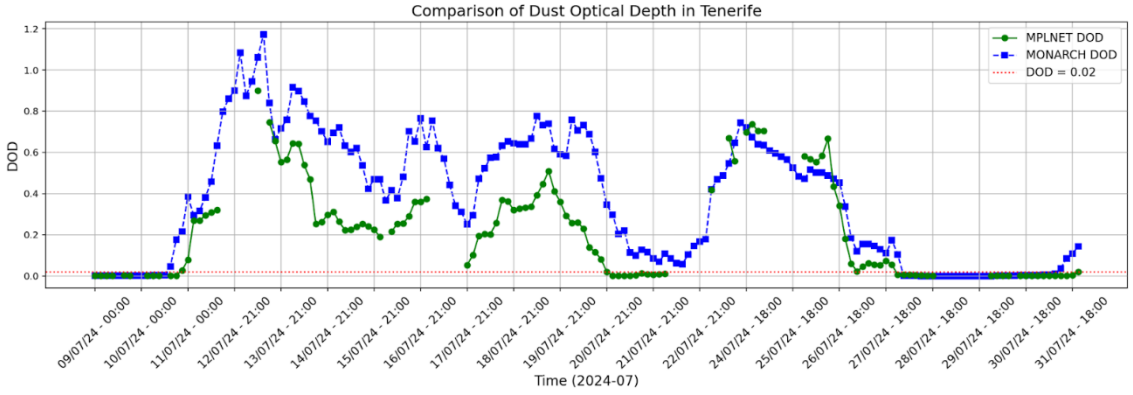

***Figure 2.6**: Time evolution of MONARCH (blue curve) and MPLNET (orange dashed curve) dust optical depth in Tenerife. The red dotted line represents the threshold we used to identify the dust events.*

Across all three sites and over the full study period, MONARCH consistently detects the presence of dust layers and replicates their approximate vertical range in the lower atmosphere (1-5 km). The underestimation or overestimation of the dust extinction may be caused by biases in the modelled dust concentration, optical properties, by uncertainties in the LIDAR dust retrieval, or by a combination of all these factors. Hence, the main focus of this comparison should be on the shape of the dust vertical distribution and its temporal evolution, the absolute extinction values being subject to a greater uncertainty. In the follow-up sections of this report, a statistical evaluation will be carried out using quantities that are not sensitive to the dust optical depth (or total extinction) but only to the vertical structure.

Due to its coarser vertical resolution, MONARCH produces less structured extinction profiles, lacking the fine-scale vertical variability observed by MPLNET, such as multiple extinction peaks or sharp gradients (e.g., Tenerife on the 14th of July 2024 and El Arenosillo on the 16th of September).

2.2. Correlation Plots

Figure 2.7 depicts the temporal variability of the correlation between MONARCH and MPLNET dust extinction coefficients. The correlation has been evaluated every 3 hours across all 13 vertical levels for those time samples for which there was a considerable load of dust (measured by the MPLNET DOD being greater than or equal to 0.02).

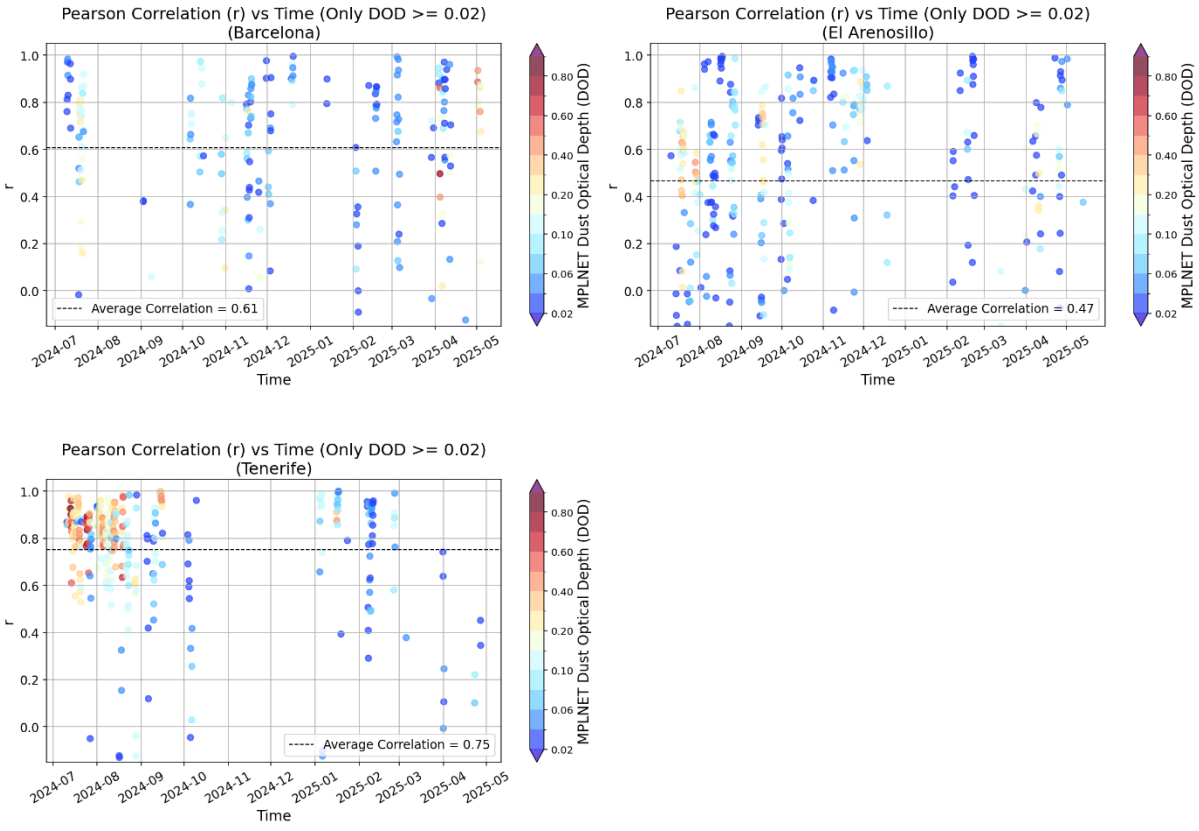

***Figure 2.7**: Time evolution of the Pearson correlation between MPLNET dust extinction and MONARCH dust*

extinction across all 13 layers. The average of the correlations is represented by a black dashed line.

A summary of the degree of similarity between modelled and observed vertical structures is shown in Table 2.1, quantified by the average Pearson correlation coefficient (r) between the two profiles, for all coincident measurements in the period of study. As previously said, to be able to realize this type of comparison, a vertical downscaling of the MPLNET high-resolution data was necessary.

***Table 2.1**: Average of the Pearson correlation coefficients between MONARCH and MPLNET dust extinction vertical profiles during dust episodes (DOD 0.02) at the three MPLNET stations.*

	Barcelona	El Arenosillo	Tenerife
Pearson Correlation Coefficient	0.61	0.47	0.75

The values in Table 2.1 indicate a moderate to strong correlation between MONARCH and MPLNET, with the highest agreement observed in Tenerife (r = 0.75).

If we only take into consideration very intense dust outbreaks ($DOD \geq 0.02$), the average correlation increases globally, reaching the values of 0.60 in Barcelona, 0.55 in El Arenosillo, and 0.84 in Tenerife.

Overall, the correlation analysis reinforces the results of the time series comparison, highlighting both the strengths of the MONARCH model in reproducing major dust events and the need for improved vertical resolution to better resolve finer vertical structures.

2.3. Average Height of the Dust Layer

To further analyse whether MONARCH realistically represents the vertical distribution of dust, we analyzed how the altitude of the dust peak, previously introduced in Section 1.3, evolves over time in both the model and lidar data.

Figures 2.8, 2.9, and 2.10 depict the time evolution of the dust layer average height in Barcelona, El Arenosillo, and Tenerife. The time series in Tenerife displays coherent dust plume structures with consistent alignment between MONARCH and MPLNET during dust events. In Barcelona, the overall correlation is moderate, but we observe inconsistent alignment between the modeled and observed dust layers. In El Arenosillo, on average, MONARCH places the dust layer at lower altitudes compared to MPLNET, particularly during more intense dust events.

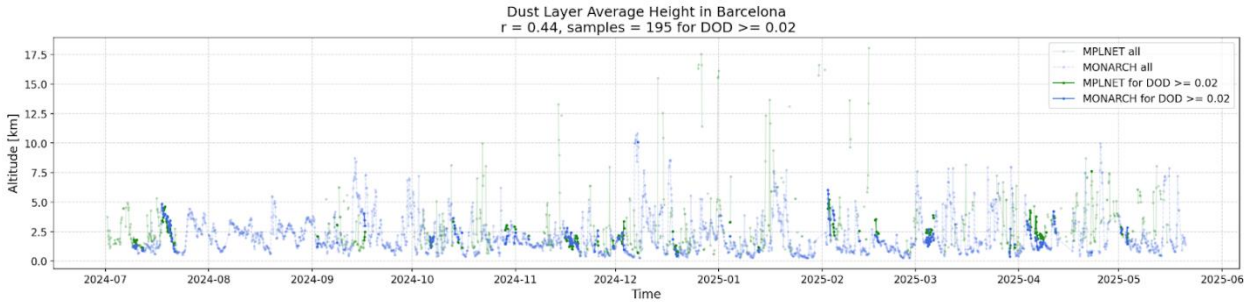

***Figure 2.8**: Time variation of the average altitude of the dust layer for MONARCH simulations and MPLNET measurements in Barcelona.*

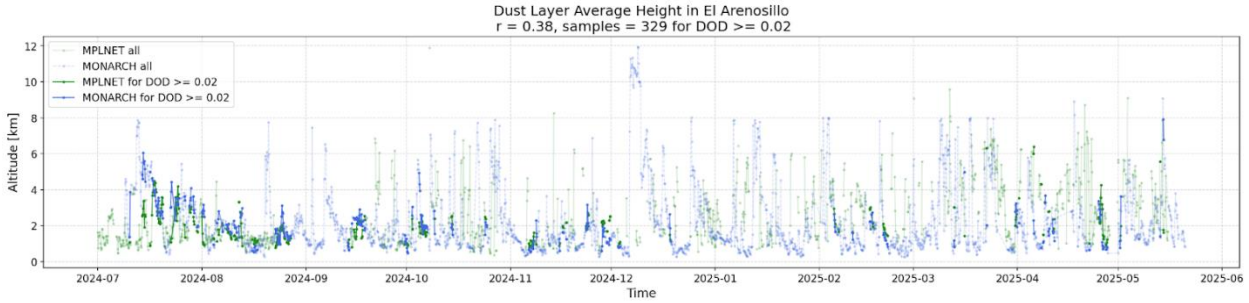

***Figure 2.9**: Time variation of the average altitude of the dust layer for MONARCH simulations and MPLNET measurements in El Arenosillo.*

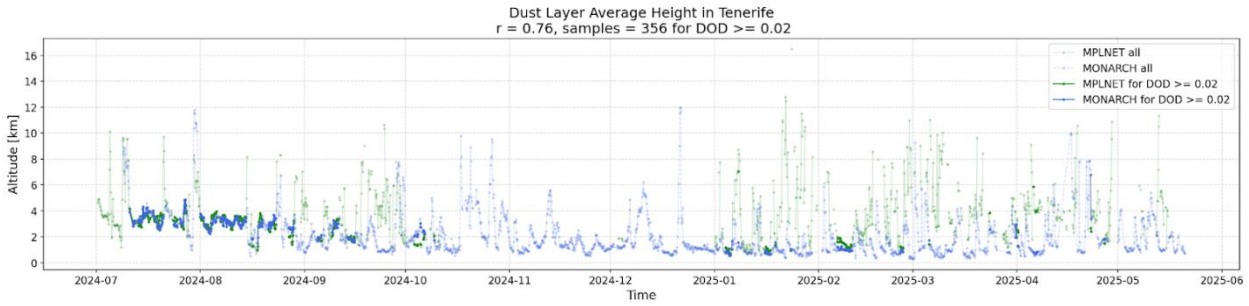

***Figure 2.10**: Time variation of the average altitude of the dust layer for MONARCH simulations and MPLNET measurements in Tenerife.*

Table 2.2 shows the correlation coefficient between MONARCH COM and MPLNET COM.

***Table 2.2**: Pearson correlation coefficient (r) and number of samples (in parentheses) between MONARCH and MPLNET average dust layer height during dust episodes ($DOD \geq 0.02$).*

	Barcelona	El Arenosillo	Tenerife
Pearson Correlation Coefficient	0.44 (195)	0.38 (329)	0.76 (356)

High correlation values are obtained in Tenerife, where we could also use more samples to evaluate the correlation. In Barcelona and El Arenosillo, we obtained lower correlation values.

This outcome strengthens the fact that MONARCH captures the dust vertical distribution reasonably well.

3. Conclusions

We compared SDS-WAS MONARCH operational forecasts of vertical dust profiles with MPLNET lidar data. We focused on three sites: Barcelona, El Arenosillo, and Tenerife, and our comparison ran from July 2024, when MONARCH's vertical profiles of dust concentration were made publicly available, to May 2025.

The first step involved the download and processing of MPLNET and MONARCH data to retrieve dust extinction profiles, which is the quantity being compared. MPLNET measurements were filtered to remove low-quality and failed retrievals. The dust component was then extracted from the total aerosol load using the POLIPHON algorithm. Some assumptions regarding the dust lidar ratio, the dust depolarization ratio, and the non-dust depolarization ratio were made. Regarding MONARCH, the vertically resolved dust extinction was calculated from the dust concentration profile, the dust load, and the dust optical depth.

The results presented in this report showed an overall good agreement between MONARCH and MPLNET. In general, we can say that the model reconstructed dust extinction vertical profiles typically coincided with MPLNET retrievals in shape, vertical extent, temporal variability, and magnitude. Nevertheless, there were scenarios of overestimation/underestimation and misplacement of the dust plumes, probably due to errors in the model's emission scheme, uncertainties in the model meteorology (e.g., wind speed or convection), or limitations in the comparison methodology. Moreover, the model did not always resolve the finer vertical structures seen in the lidar data due to its coarser resolution.

The Pearson correlation coefficient was also exploited to compare the model against lidar data. The correlation was computed over the entire period, focusing on dust transport episodes (identified by the DOD being greater than or equal to 0.02). The outcome showed a moderate to high average correlation in the three sites, enforcing the good agreement already seen in the vertical profiles.

As the last method of evaluation, we used the average height of the dust layer. We calculated the dust layer's center of mass over the whole time period of both MPLNET and MONARCH, and we examined the correlation during dust events. The results showed an overall good agreement (with the highest correlation reached in Tenerife), even if some spatial and temporal discrepancies were observed.

It is important to note that the availability of MPLNET data was limited during the study period. Before applying the 3-hourly temporal averaging, less than 40% of the original MPLNET extinction profiles passed the quality screening criteria. This data sparsity, especially during certain periods, calls for an extension of this analysis in time in the future.

This evaluation highlights both strengths and limitations of the MONARCH operational forecast for vertical dust profiles. The model reliably captures the presence, shape, and temporal variability of dust layers. However, the analysis also underscores some key limitations. The coarse vertical resolution of the products of the model limits its ability to resolve fine-scale

structures such as multi-layered dust events, which are often observed by lidar. In some cases, the model underestimates the altitude or intensity of the dust layer, which may be linked to uncertainties in the components of the models. Key model parameters of the model's dust emissions and aerosol modules (e.g., wet and dry deposition, aerosol optics or boundary layer diffusion parameters, etc) are set to match observed aerosol optical depth from satellite or ground-based sources, but they may not always be optimized for representing vertical structure.

This evaluation could be further improved and extended by comparing MONARCH with other regional or global dust models, such as those from the SDS-WAS or CAMS ensemble, to place its performance and evaluation in a larger modeling context.

5. References

Ansmann, A., Rittmeister, F., Engelmann, R., Basart, S., Jorba, O., Spyrou, C., Remy, S., Skupin, A., Baars, H., Seifert, P., Senf, F., & Kanitz, T. (2017). Profiling of Saharan dust from the Caribbean to western Africa – Part 2: Shipborne lidar measurements versus forecasts. *Atmospheric Chemistry and Physics, 17*, 14987–15006. https://doi.org/10.5194/acp-17-14987-2017

Ansmann, A., Mamouri, R.-E., Hofer, J., Baars, H., Althausen, D., & Abdullaev, S. F. (2019). Dust mass, cloud condensation nuclei, and ice-nucleating particle profiling with polarization lidar: Updated POLIPHON conversion factors from global AERONET analysis. *Atmospheric Measurement Techniques, 12*, 4849–4865. https://doi.org/10.5194/amt-12-4849-2019

Badia, A., & Jorba, O. (2015). Gas-phase evaluation of the online NMMB/BSC-CTM model over Europe for 2010 in the framework of the AQMEII-Phase2 project. *Atmospheric Environment, 115*, 657-669.

Badia, A., Jorba, O., Voulgarakis, A., Dabdub, D., Pérez García-Pando, C., Hilboll, A., Gonçalves, M., & Janjic, Z. (2017). Description and evaluation of the Multiscale Online Nonhydrostatic AtmospheRe CHemistry model (NMMB-MONARCH) version 1.0: gas-phase chemistry at global scale. Geoscientific Model Development, 10, 609-638. https://doi.org/10.5194/gmd-10-609-2017

Campbell, J. R., Hlavka, D. L., Welton, E. J., Flynn, C. J., Turner, D. D., Spinhirne, J. D., Scott , V. S., III, & Hwang, I. H. . (2002). Full-Time, Eye-Safe Cloud and Aerosol Lidar Observation at Atmospheric Radiation Measurement Program Sites: Instruments and Data Processing. Journal of Atmospheric and Oceanic Technology, 19(4), 431-442. https://doi.org/10.1175/1520-0426(2002)019<0431:FTESCA>2.0.CO;2

Di Tomaso, E., Schutgens, N. A. J., Jorba, O., & Pérez García-Pando, C. (2017). Assimilation of MODIS Dark Target and Deep Blue observations in the dust aerosol component of NMMB/BSC-CTM version 1.0. Geoscientific Model Development, 10, 1107-1129. https://doi.org/10.5194/gmd-10-1107-2017

Di Tomaso, E., Escribano, J., Basart, S., Ginoux, P., Macchia, F., Barnaba, F., Benincasa, F., Bretonnière, P.-A., Buñuel, A., Castrillo, M., Cuevas, E., Formenti, P., Gonçalves, M., Jorba, O., Klose, M., Mona, L., Montané Pinto, G., Mytilinaios, M., Obiso, V., Olid, M., Schutgens, N., Votsis, A., Werner, E., & Pérez García-Pando, C. (2022). The MONARCH high-resolution reanalysis of desert dust aerosol over Northern Africa, the Middle East and Europe (2007–2016). Earth System Science Data, 14, 2785-2816. https://doi.org/10.5194/essd-14-2785-2022

Escribano, J., Di Tomaso, E., Jorba, O., Klose, M., Gonçalves Ageitos, M., Macchia, F., Amiridis, V., Baars, H., Marinou, E., Proestakis, E., Urbanneck, C., Althausen, D., Bühl, J., Mamouri, R.-E., & Pérez García-Pando, C. (2022). Assimilating spaceborne lidar dust extinction can improve dust forecasts. Atmospheric Chemistry and Physics, 22, 535-560. https://doi.org/10.5194/acp-22-535-2022

Haustein, K., Pérez, C., Baldasano, J. M., Jorba, O., Basart, S., Miller, R. L., Janjic, Z., Black, T., Nickovic, S., Todd, M. C., Washington, R., Müller, D., Tesche, M., Weinzierl, B., Esselborn, M., & Schladitz, A. (2012). Atmospheric dust modeling from meso to global scales with the online NMMB/BSC-Dust model – Part 2: Experimental campaigns in Northern Africa. Atmospheric Chemistry and Physics, 12, 2933-2958. https://doi.org/10.5194/acp-12-2933-2012

Janjic, Z., & Gall, L. (2012). Scientific documentation of the NCEP nonhydrostatic multiscale model on

the B grid (NMMB). Part 1 Dynamics.

Jorba, O., Dabdub, D., Blaszczak-Boxe, C., Pérez, C., Janjic, Z., Baldasano, J. M., Spada, M., Badia, A., & Gonçalves, M. (2012). Potential significance of photoexcited NO2 on global air quality with the NMMB/BSC chemical transport model. Journal of Geophysical Research: Atmospheres, 117. https://doi.org/10.1029/2012JD017730

Klose, M., Jorba, O., Gonçalves Ageitos, M., Escribano, J., Dawson, M. L., Obiso, V., Di Tomaso, E., Basart, S., Montané Pinto, G., Macchia, F., Ginoux, P., Guerschman, J., Prigent, C., Huang, Y., Kok, J. F., Miller, R. L., & Pérez García-Pando, C. (2021). Mineral dust cycle in the Multiscale Online Nonhydrostatic Atmosphere Chemistry model (MONARCH) version 2.0. Geoscientific Model Development, 14, 6403-6444. https://doi.org/10.5194/gmd-14-6403-2021

Mamali, D., Marinou, E., Sciare, J., Pikridas, M., Kokkalis, P., Kottas, M., Binietoglou, I., Tsekeri, A., Keleshis, C., Engelmann, R., Baars, H., Ansmann, A., Amiridis, V., Russchenberg, H., & Biskos, G. (2018). Vertical profiles of aerosol mass concentration derived by unmanned airborne in situ and remote sensing instruments during dust events. Atmospheric Measurement Techniques, 11, 2897-2910. https://doi.org/10.5194/amt-11-2897-2018

Mona, L., Amodeo, A., Pandolfi, M., & Pappalardo, G. (2006). Saharan dust intrusions in the Mediterranean area: Three years of Raman lidar measurements. Journal of Geophysical Research, 111, D16203. https://doi.org/10.1029/2005JD006569

Pérez, C., Haustein, K., Janjic, Z., Jorba, O., Huneeus, N., Baldasano, J. M., Black, T., Basart, S., Nickovic, S., Miller, R. L., Perlwitz, J. P., Schulz, M., & Thomson, M. (2011). Atmospheric dust modeling from meso to global scales with the online NMMB/BSC-Dust model – Part 1: Model description, annual simulations and evaluation. Atmospheric Chemistry and Physics, 11, 13001-13027. https://doi.org/10.5194/acp-11-13001-2011

Proestakis, E., Amiridis, V., García-Pando, C. P., Tsyro, S., Griesfeller, J., Gkikas, A., Georgiou, T., Ageitos, M. G., Escribano, J., Myriokefalitakis, S., Masso, E. B., Di Tomaso, E., Basart, S., Stuut, J.-B. W., & Benedetti, A. (2025). Quantifying dust deposition over the Atlantic Ocean. Earth System Science Data Discuss. [preprint]. https://doi.org/10.5194/essd-2025-43

Spada, M., Jorba, O., Pérez García-Pando, C., Janjic, Z., & Baldasano, J. M. (2013). Modeling and evaluation of the global sea-salt aerosol distribution: Sensitivity to size-resolved and sea-surface temperature dependent emission schemes. Atmospheric Chemistry and Physics, 13(23), 11735-11755.

Spada, M. (2015). Development and evaluation of an atmospheric aerosol module implemented within the NMMB/BSC-CTM.

Tesche, M., A. Ansmann, D. Müller, D. Althausen, R. Engelmann, V. Freudenthaler, and S. Groß (2009), Vertically resolved separation of dust and smoke over Cape Verde using multiwavelength Raman and polarization lidars during Saharan Mineral Dust Experiment 2008, J. Geophys. Res., 114, D13202, doi:10.1029/2009JD011862.

Welton, E. J., Campbell, J. R., Spinhirne, J. D., & Scott, V. S. III. (2001). Global monitoring of clouds and aerosols using a network of micropulse lidar systems. Proceedings of SPIE 4153, Lidar Remote Sensing for Industry and Environment Monitoring. https://doi.org/10.1117/12.417040

Welton, E. J., & Campbell, J. R. (2002). Micropulse Lidar Signals: Uncertainty Analysis. Journal of Atmospheric and Oceanic Technology, 19(12), 2089-2094. https://doi.org/10.1175/1520-0426(2002)019<2089:MLSUA>2.0.CO;2

Xian, P., Reid, J. S., Hyer, E. J., Sampson, C. R., Rubin, J. I., Ades, M., Asencio, N., Basart, S.,

Benedetti, A., Bhattacharjee, P. S., Brooks, M. E., Colarco, P. R., da Silva, A. M., Eck, T. F., Guth, J., Jorba, O., Kouznetsov, R., Kipling, Z., Sofiev, M., Pérez García-Pando, C., Pradhan, Y., Tanaka, T., Wang, J., Westphal, D. L., Yumimoto, K., & Zhang, J. (2019). Current state of the global operational aerosol multi-model ensemble: An update from the International Cooperative for Aerosol Prediction (ICAP). *Quarterly Journal of the Royal Meteorological Society, 145*, 176-209. https://doi.org/10.1002/qj.3497